International Journal of Engineering Applied Sciences and Technology, 2020
Vol. 5, Issue 8, ISSN No. 2455-2143, Pages 211-218
Published Online December 2020 in IJEAST (http://www.ijeast.com)

DESIGN, CFD ANALYSIS AND PERFORMANCE EVALUATION OF COMBINED STEAM EJECTOR SINGLE EFFECT LIBR/H_2O ABSORPTION REFRIGERATION SYSTEM

Munawar Nawab Karimi
Department of Mechanical Engineering,
Jamia Millia Islamia, New Delhi, India

Salem Alabd Mohamed
Department of Mechanical Engineering,
Jamia Millia Islamia, New Delhi, India

Abstract— **The objective of this work is to develop the efficiency of vapour absorption system by addition the steam ejector cycle. Computational fluid dynamics (CFD) is a numerical implement that is greatly accurate to simulate a high number of applications and developments. The CFD analysis has appeared as a viable skill to provide dynamic and efficient design solutions. In this work a CFD analysis concentrate on the mathematical simulation of the operating of a steam ejector to develop the Efficiency of vapour absorption cycle using LiBr/H_2O as a working refrigerant for this system and operating under steady-state conditions. The overall design steam ejector technique that follows ASHRAE and ESDU recommended are considered in this study, throat nozzle diameter of 4.13 mm, and suction maxing chamber diameter of 10 mm. The effect of different operational settings on the performance of the steam ejector operating in combination with a single effect absorption system was measured. The geometrical model and meshing is done with solid works and ANSYS FLUENT solver is used for the analysis. In this research study, development to the system is achieved by utilizing the potential kinetic energy of the ejector to enhance refrigeration efficiency. The effects of the entrainment ratio of the ejector, primary and secondary operating temperature, on the condition condenser pressure and temperature and system performance have been studied. The results showed that the entrainment ratio is found to increase with the decrease of secondary pressure (evaporator pressure) and consequently, the entrainment ratio is also found to increase with increase of generator temperature keeping the evaporator temperature and condenser pressure constant. The entrainment ratio does not vary much with the condenser pressure until the critical condenser pressure. The COP of the established system is developed by up to 45% compared with that Basic system at the given condition.**

Keywords— LiBr/H_2O absorption system, Steam Ejector cycle, Enhance COP, CFD

I. INTRODUCTION

Since several decades, the research in the field of ARS has been oriented towards improvement in the performance (or COP) of the overall system. Efforts have been utilized to focus on individual components and enhance their performance to achieve improved system behaviour in total. In some of the recent research work, attempts are made to enhance the ARS performance by coupling with ejector system [1]. Presented that the integration of ejector system with basic absorption cycle has evolved as a promising approach as it has uplifted the COP of the basic VAS from the range of 0.2-0.6 to the range 0.5-0.85, [2] The ejector can operate working fluid with low boiling points. The ejector coupled VAS can be used to drive the refrigerant from the thermal energy at temperature above 333K, which is easily available at the absorber of the VAS. Due to these advantages, several researches on the Ejector Refrigeration System (ERS) has been reported in the recent literature. [3]. tried enhancing the system performance by developing an ERS model with incorporation of an ejector between the condenser and the steam generator,[4]. Proposed compression enhanced approach using booster sub-cycle to increase the COP of Ejector Refrigeration System, [5]. proposed application of jet pump in ERS to bring down the backpressure of the ejector, thereby increasing the entrainment ratio and the COP of the entire system. [6,7], demonstrated the performance enhancement of ERS by further integration of a flash tank to the system. Next, [8] Investigated modification of ejector system coupled with flash tank by utilizing waste heat through rearrangement of the streamlines at the solution heat exchanger and incorporation of RHE.

Later, [9] Reported that the effectiveness of steam ejector could be optimized by removing the booster on high pressure of the refrigerant streamline side by changing the steam ejector nozzle shape or diameter and allowing the secondary how flows from evaporator side of the ejector to work only under middle pressure of the flash tank with NH_3–H_2O as its working pairs fluid. [10] Performed thermodynamic analysis of single-stage absorption cycle coupled with ejector, to

International Journal of Engineering Applied Sciences and Technology, 2020
Vol. 5, Issue 8, ISSN No. 2455-2143, Pages 211-218
Published Online December 2020 in IJEAST (http://www.ijeast.com)

investigate the effects of different parameters like the ejector's entrainment ratio, and the operating temperature on the thermal loads and the system performance. The results revealed that the COP of the ERS is higher than that of the basic ARS by 60%. The cooling capacity of the system improves with increase in the evaporator temperature and the entrainment ratio. Moreover, the thermal load of the condenser as well as of the evaporator increase with generator and evaporator temperature, while it decreases with increase in the condenser temperature.

This research paper deals with the theoretical and CFD analysis of single stage LiBr/H_2O ERS. The theoretical formulations have been derived from the mathematical model of S. A.

II. DESCRIPTION OF COMBIND LIBR/ H_2O ABSORPTION- EJECTOR SYSTEM

The cycle has four important components namely, i). a generator, ii). a condenser, iii). an evaporator, and iv). An absorber. The absorber cycle operates between two pressure levels: low pressure acting at evaporator-absorber side, and high pressure acting at condenser- generator side. When ejector is used in combination with the absorption cycle, it is located between the generator and the condenser, as schematically shown in **Error! Reference source not found.**.

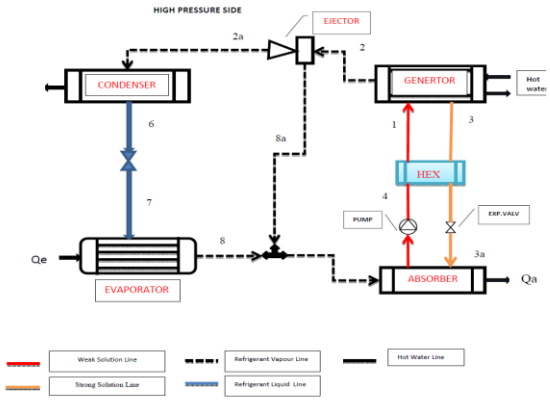

Fig: 1. System schematic of single effect LiBr/H_2O combined vapour absorption – ejector refrigeration system

When the heat from the heat source is supplied to the LiBr/water solution in the generator, the water gets evaporated. The high-pressure water vapour (8a) then moves to the ejector, after which it reaches in the mixing chamber where it gets mixed with the low-pressure vapour (8a) approaching from the evaporator. The mixture next passes through the diffuser and enters the condenser. On the other side, the saturated LiBr/water solution (brine) inside the absorber (4) at low pressure is pumped to the generator at high pressure (1), where it the water is separated and a strong LiBr solution is left back. The strong solution left after vaporization of water, travels through the heat exchanger, throttled to low-pressure solution and finally sprayed onto the absorber (3a).

The ejector of comprises of a converging-diverging nozzle as shown in Figure 1. which is responsible for producing entrainment effect. The primary fluid from the generator enters the nozzle at subsonic velocity and leaves it at supersonic state. Due to this the kinetic energy of the primary fluid is raised while the pressure drops down. This pressure difference between the primary fluid at nozzle exit and the secondary fluid at inlet produces the entrainment effect while secondary fluid is absorb through the inlet of ejector because of the vacuum pressure that happened in nozzle, the mixture of primary and secondary fluid flow through the mixing zone at constant pressure until it reaches the diffuser at subsonic velocity. The mixture is compressed back to the prescribed condenser pressure while passing through the diffuser.

III. THERMODYNAMIC ANALYSIS

In order to predict the performance of vapour absorption system combined with ejector, the mathematical framework, used by [11] has been deployed in the present study. Using this model, the effect of entrainment ratio of the ejector on the system performance has been examined. According to this model, the system performance can be suitably assessed in terms of COP and the ejector's Entrainment Ratio (ER). The mathematical expression for COP and ER are provided in Eq. (1) and Eq. (2):

$$COP = \frac{Q_E}{Q_g + W_p} \quad (1)$$

$$ER = \frac{\dot{m}_s}{\dot{m}_p} \quad (2)$$

IV. DESIGN AND ANALYSIS OF THE EJECTOR

A. *Ejector Geometry*

In a combined vapour absorption-ejector system, the role of ejector is highly crucial in determining the overall system performance. This necessitates an accurate selection of geometry, design and analysis. In vast of the research work, use of the recommended specifications of ASHRAE and ESDU for ejector configuration have been reported both for geometrical dimensions and non-dimensional parameters, [12,13], the same recommendations have also been followed in the present work during CFD simulation one by one until a near-optimum geometry is obtained which ensures maximum entrainment ratio at the desired operating conditions. **Error! Reference source not found.** shows the ejector geometry of the so obtained model.

International Journal of Engineering Applied Sciences and Technology, 2020
Vol. 5, Issue 8, ISSN No. 2455-2143, Pages 211-218
Published Online December 2020 in IJEAST (http://www.ijeast.com)

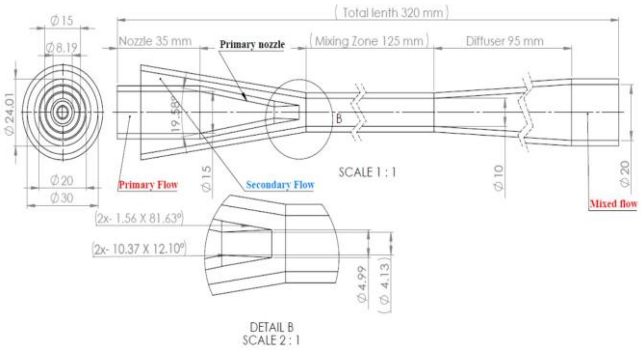

Fig: 2. Schematic diagram of the ejector geometries dimensions as the base model.

14.0 workbench packages was used for the pre-processing, post processing and solving of this compressible flow problem. The geometry of the ejector was designed in Design Modeller, the meshing was done in Ansys meshing and then it is solved in Ansys Fluent. **Error! Reference source not found.** shows the design lamina for the geometry the geometry was modeled in 3D dimensions, using the thickness of x value to be 2mm, and therefore corresponding dimensions of y & z. The geometry made is shown in Figure 1:

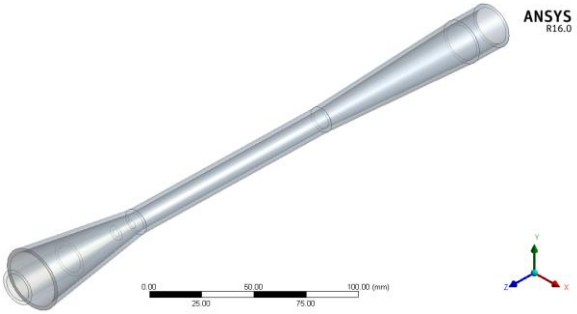

Figure 1: Isometric view of the ejector geometry

B. Ejector Meshing

Error! Reference source not found. shows the geometry of the ejector made in ANSYS Design Modeller. After the geometry of the ejector is finished, it is meshed, yielding 611317 number of elements and 114906 number of nodes. In our case, Quad mesh was employed using solver preference fluent, high smoothing, slow transition, initial size seed active assembly.

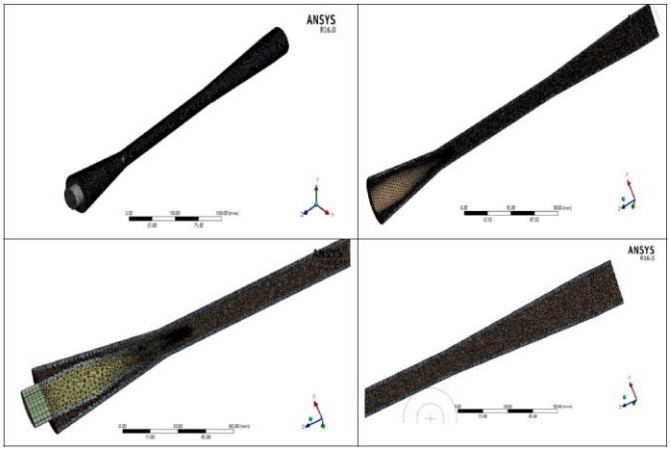

Fig: 4. Meshing model of 3D ejector geometry in different view

Now as the proper mesh was generated using the advancing front method, the mesh had one inlet primary flow, one inlet secondary flow, one outlet mixture flow outlet, inner tube nozzle wall, outer tube solid and fluid domain as the named selections. Now the mesh was to be solved and so was imported in Fluent.

The analysis setup based on k-epsilon (2eq), realizable and enhanced wall treatment, three cell zone condition nozzle inner tube and outer tube solid materials (aluminium), primary and secondary fluid flow (water vapour) at different mass flow rate and temperature corresponding to the single effect vapour absorption system, J.M. Chang et al. (1999); B.J.Huang et al. (2013).

C. CFD Implementation

For performing CFD analysis, a two cell zone conditions of the solid and fluid flow domains were used to obtain accurate result. The ejector assembly was imported in ANSYS Fluent v.16 for mesh examination and consequently, for the CFD implementation. The pressure-based solver with velocity formulation and steady state type implicit formulation was used to solve the governing equations for continuity, momentum, and energy and species transport concurrently, on the account that the flow is compressible. Next, the principal equations for supplementary scalars such as turbulence will be solved. Although steady state is applied, from the standpoint of numerical solutions, for steady-state assumption with travelling shocks, implicit formulation may be more efficient. In order to automatically refine the meshes in the regions of large temperature gradients and converge the analysis, the temperature gradient adaptation was set. Viscous model using realizable k-epsilon (2eq) and enhanced wall treatment, while, the pressure- velocity coupling for solution methods was selected. Spatial discretization system is solved with Least Squares Cell-based gradient calculations, the model initialized as hybrid solution initialization. This is the most recommended turbulence model for turbulent compressible

International Journal of Engineering Applied Sciences and Technology, 2020
Vol. 5, Issue 8, ISSN No. 2455-2143, Pages 211-218
Published Online December 2020 in IJEAST (http://www.ijeast.com)

flows, [14,15], Single-phase flow assumption is considered since both flow inlet conditions are in the vapor states; although phase change can happen, it is likely to happen temporarily in slight limited areas and it's negligible.

Fluid flow through the ejector can be measured compressible, turbulent, steady-state and pressure based. The Navier-Stokes continuity, momentum and energy equations afford the establishment in CFD simulation analysis of fluid flow movement. The average values of flow quantities including velocity are usually determined by time averaging over large intervals, sifting out small variations, but small enough to maintain large scale time variations. This results in continuity, momentum, and energy and species transport concurrently equations. The subsequent equations are written in Cartesian tensor form as [16]:

$$\frac{\partial \rho}{\partial t} + \frac{\partial}{\partial x_i}(\rho u_i) = 0 \quad (3)$$

$$\frac{\partial}{\partial t}(\rho u_i) + \frac{\partial}{\partial x_j}(\rho u_i u_j) = -\frac{\partial p}{\partial x_i} + \frac{\partial \tau_{ij}}{\partial x_j} \quad (4)$$

$$\tau_{ij} = \mu_{eff}\left(\frac{\partial u_i}{\partial x_j} + \frac{\partial u_j}{\partial x_i}\right) - \frac{2}{3}\mu_{eff}\frac{\partial u_k}{\partial x_k}\delta_{ij} \quad (5)$$

$$\frac{\partial}{\partial_t}(\rho E) + \frac{\partial}{\partial x_i}\left(u_i(\rho E + P)\right) = \vec{\nabla}.\left(\alpha_{eff}\frac{\partial T}{\partial x_i}u_j(\tau_{ij})\right) \quad (6)$$

A. Boundary Conditions

In order to conduct the CFD analysis of ejector based single effect LiBr/water vapour absorption refrigeration cycle, the following operating conditions were chosen for air conditioning purpose:

- Evaporator temperature: $10°C$
- Condenser temperature: $\sim 40°C$
- Generator temperature: $97°C$.

The temperatures of generator, condenser and evaporator (T_g, T_C, T_E) were varied under preferred range to evaluate the geometry at off-design conditions:

- T_g range: $89 - 97°C$
- T_C range: $40 - 45°C$, and
- T_E range: $2 - 10°C$.

The 'pressure–velocity' boundary conditions are mandatory for primary and secondary flows as well as for mixed flow at diffuser outlet.

V. RESULTS AND DISCUSSION

The results of the analysis have been presented in this section. The static pressure, temperature, and velocity contours of the steam ejector have been plotted in **Error! Reference source not found.**, **Error! Reference source not found.**, and **Error! Reference source not found.**. The same boundary conditions as applied in [17,18], were taken at the inlets. The condenser pressure (or back pressure), P_C= 7373.39 Pa was taken which corresponds to a preferred saturation solution temperature, T_C=314K. The mass flow rate is 0.0212kg/s, and the outlet temperature is 370K, which implies that the vapour leaving the generator outlet is in superheated state. There are approximately 611317 elements in the computational domain out of which only very few exist in the primary nozzle and mixing zone, and hence, according to the statistical perception, the flow is considered mainly a single phase.

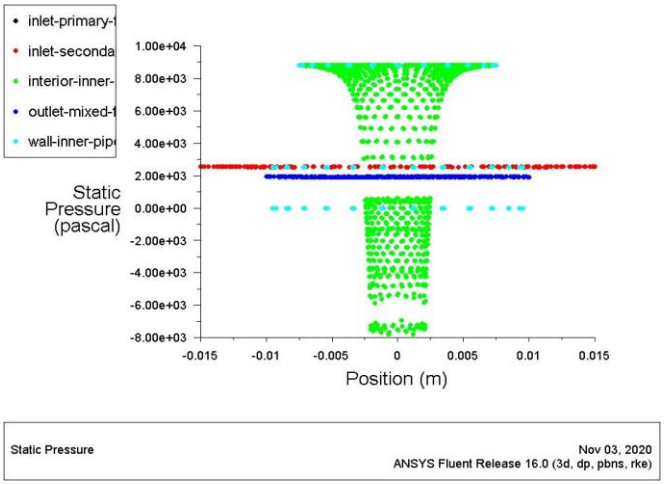

Fig: 5. Static pressure plot of Computational Elements

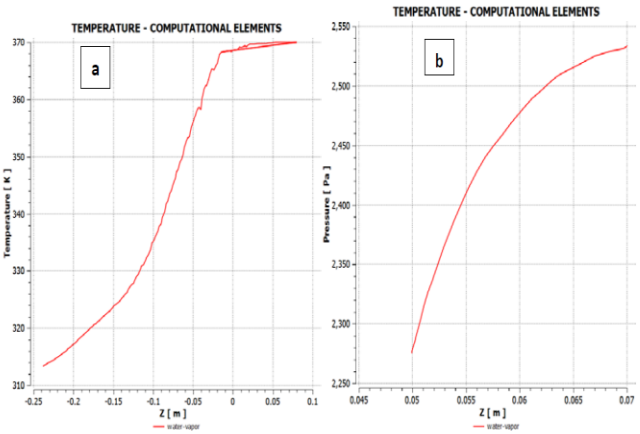

Fig: 6. (a) Temperature and (b) pressure plot of Computational Elements

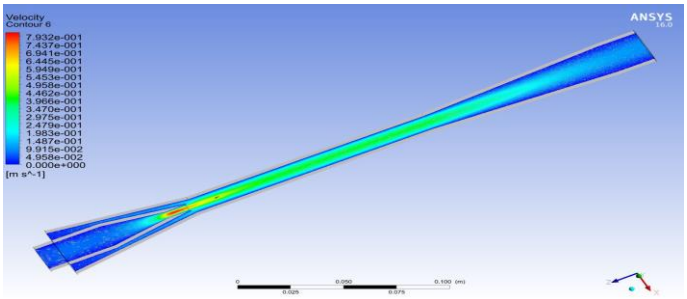

International Journal of Engineering Applied Sciences and Technology, 2020
Vol. 5, Issue 8, ISSN No. 2455-2143, Pages 211-218
Published Online December 2020 in IJEAST (http://www.ijeast.com)

Fig: 7. Profile velocity contour and presence of oblique suddenness.

The contours of the flow velocity shown in **Error! Reference source not found.** depicts a close ideal ejector process because these contour determines the presence of a sequences of oblique suddenness surfs in primary fluid flow, downstream the nozzle exit and a single shockwave in the combined flow at the diffuser entry, [18,19]. As a result, an effective recompression is produced in the combined fluid flowing inside the diffuser to the desired outlet pressure, P_C. The occurrence of shock can also be observed in the pressure contour profile plotted in **Error! Reference source not found.** and the density profile in **Error! Reference source not found.**. The shock waves are incorporated by applying quick deviations in the flow pressure at constant densities.

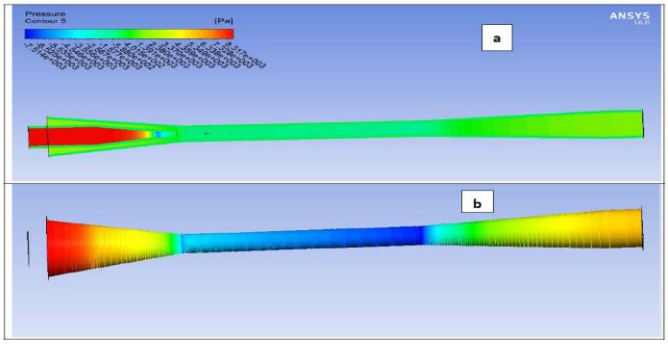

Fig: 8. (a) Contours of primary and secondary flow and (b) outer of fluid domain Pressure (Pa)

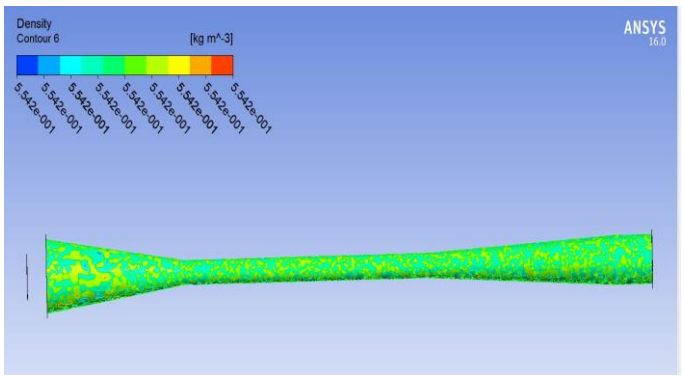

Fig: 9. Contours of Density in (kg/m^3).

Error! Reference source not found. shows the temperature contours of the ejector at two different inlet temperatures of generator (primary inlet) and evaporator (secondary inlet). **Error! Reference source not found.**(a) displays the temperature contour at boundary condition $T_P = 97°C$, $T_s = 10°C$, while **Error! Reference source not found.**(b) displays the temperature contour at boundary condition $T_P = 89°C$, $T_s = 2°C$. It is observed that when we decreasing the temperature input of primary flow and keeping the secondary flow temperature as constant, the outlet mixture flow after passing the ejector is slightly reduce in condenser temperature and pressure outlet but when we increasing the temperature input of the secondary flow temperature and keeping the primary flow input as constant the condenser temperature (outlet mixing flow) is more better optimize, and that's will improve the overall performance system.

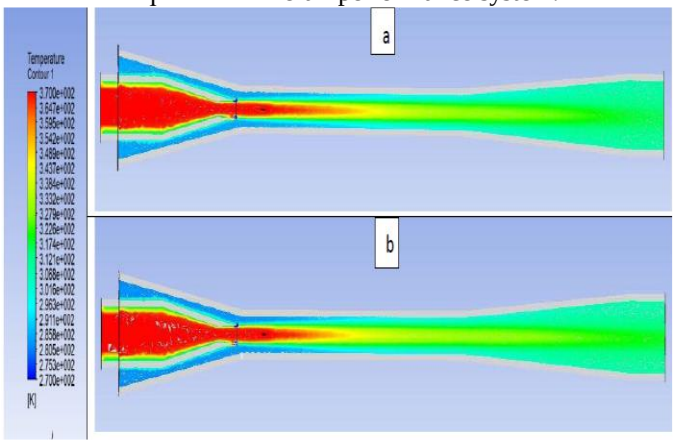

Figure 1: Temperature contour view of steam ejector at boundary conditions: (a) $T_P = 97°C$, $T_s = 10°C$ and, (b) $T_P = 89°C$, $T_s = 2°C$

Error! Reference source not found. shows the profile of turbulence kinetic energy of steam ejector at two different values of inlet temperatures of generator (primary inlet) and evaporator (secondary inlet). **Error! Reference source not found.**(a) displays the energy contour at boundary condition $T_P = 97°C$, $T_s = 10°C$, while **Error! Reference source not found.**(b) displays the energy contour at boundary condition $T_P = 89°C$, $T_s = 2°C$. It is observed that the Figure 11(a) which with $97°C$, $10°C$ primary and secondary temperature input respectively has highest turbulence kinetic energy at average value 168 J.k^{-1}, and figure 11(b) with $89°C, 2°C$ have lowest kinetic energy at around 156 J.k^{-1}.

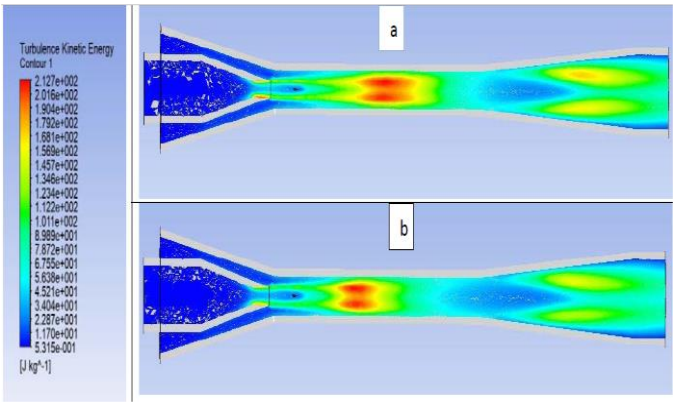

Figure 2: Turbulent kinetic energy contour view of steam ejector at boundary conditions: (a) $T_P = 97°C$, $T_s = 10°C$ and, (b) $T_P = 89°C$, $T_s = 2°C$

International Journal of Engineering Applied Sciences and Technology, 2020
Vol. 5, Issue 8, ISSN No. 2455-2143, Pages 211-218
Published Online December 2020 in IJEAST (http://www.ijeast.com)

The influence of inlet and outlet operational settings can also be observed from the results provided in Table 1 and **Error! Reference source not found.**. It can be drawn from there that increase in the entrainment ratio leads to decrease in the secondary fluid pressure (or evaporator pressure) when T_E is lower, while it results in reduction of primary fluid pressure when T_g smaller.

The second condition results in some reverse flow through the secondary inlet at T_g= 362K, thereby highlighting the ejector drawback.

Table 1: The Effect of Primary Pressure (Condenser Pressure) on Entrainment Ratio

	Boundary Conditions				Results				
	P_p (Pa)	P_s(Pa)	T_p, (K)	T_s (K)	T_c(K)	P_d(Pa)	m_s, (kg/s)	m_p, (kg/s)	ER
1	7373.39	1227.6	370	283	316.29	505.132	0.003171	0.001677	0.5288
2	6620.10	1227.6	368	283	316.72	470.178	0.003099	0.001586	0.5117
3	5940.23	1227.6	366	283	315.46	433.600	0.003014	0.001497	0.4966
4	5320.47	1227.6	364	283	314.27	400.455	0.002933	0.001411	0.4810
5	4750.54	1227.6	362	283	313.10	371.155	0.002862	0.001328	0.4640

It is also worth mentioning according to Table 1 data that the primary mass flow rate (m_p) falls with decreasing entrainment ratio because of the insufficient pressure, required to drive the primary fluid through the nozzle throat of the ejector. By reducing the primary pressure and keeping the secondary pressure constant as input boundary condition for the simulation we observed that the entrainment ratio dropped, but in Table 6.2 shows that by reduce the secondary pressure input and keeping the primary pressure constant, the entrainment ratio increase.

Table: 2. The Effect of Secondary Pressure (Evaporator Pressure) on Entrainment Ratio

	Boundary Conditions				Results				
	P_s (Pa)	P_p(Pa)	T_s, (K)	T_p (K)	T_c(K)	P_d(Pa)	m_s, (kg/s)	m_p, (kg/s)	ER
1	1227.6	7373.39	283	370	316.29	505.132	0.003171	0.001677	0.5288
2	1072	7373.39	281	370	319.41	517.694	0.002963	0.001669	0.5632
3	935	7373.39	279	370	318.19	498.278	0.002898	0.001676	0.5783
4	813	7373.39	277	370	314.43	471.052	0.003014	0.001702	0.5646
5	705	7373.39	275	370	313.28	450.369	0.002973	0.001708	0.5745

The CFD model was initially used to improve verify the performance of single ejector geometry, operating with lithium bromide water for absorption refrigeration system, over a wide range of operating temperature.

The generator temperature (primary flow) was varied in the range '$89-97°C$' in $2°C$ increments, while the evaporator temperature (secondary flow) was varied in the range '$2-10°C$' in step of $2°C$. The temperature at the outlet of the mixing chamber was in the range '$40-45°C$'. The summary of the results obtained using CFD is presented in **Error! Reference source not found.**. The entrainment ratio at the critical condenser pressure is shown where the purpose of entrainment ratio was reduced to 95% of the critical operation value.

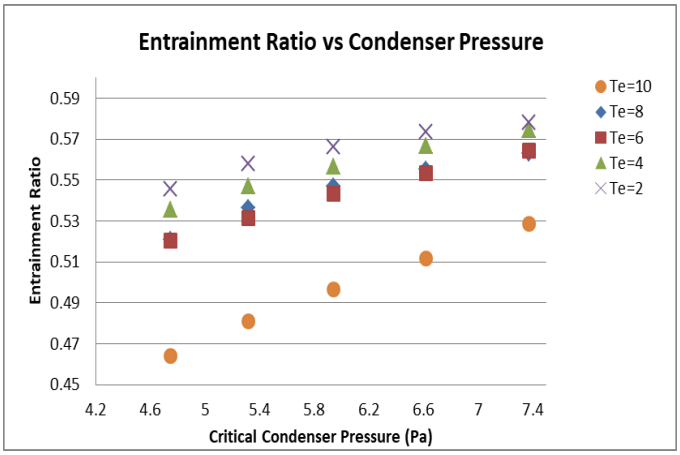

Fig: 12. Summary of performance estimates of the ejector used in the current study

According to the results tabulated in Table 1, as the generator temperature reduces, the condenser pressure (P_C) as well as the entrainment ratio (ER) also fall down, while they have opposite relation with evaporator temperature, i.e. when evaporator temperature falls, then both the condenser pressure and the entrainment ratio increase, as descriptive in **Error! Reference source not found.**.

Error! Reference source not found. shows the comparative view of system performance in case of modified (ejector based) and basic cycles, under the abovementioned range of evaporator temperature. It can be seen that by addition of ejector to the basic cycle, the COP is enhanced by 45% for throughout the selected temperature range of evaporator. The increase in COP is because of the steam ejector design, responsible to create high discharge pressure, thereby improving the entrainment effect and compress the suction load.

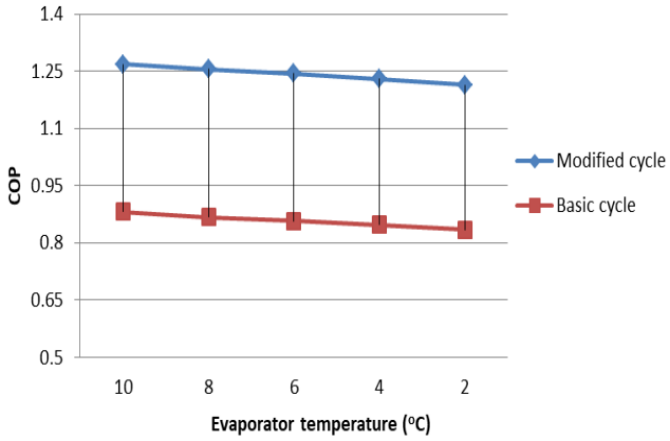

International Journal of Engineering Applied Sciences and Technology, 2020
Vol. 5, Issue 8, ISSN No. 2455-2143, Pages 211-218
Published Online December 2020 in IJEAST (http://www.ijeast.com)

Fig: 13 Comparative view of system COP for modified (ejector based) and basic cycles under different evaporators temperatures

VI. CONCLUSION

In this research study, CFD analysis of steam ejector coupled with single effect vapour absorption system has been conducted at different generator and evaporator temperatures. The throat nozzle diameter of the ejector was taken as 4.13 mm while the suction mixing chamber diameter was taken as 10 mm. The main findings of the analysis are as follow:

- The entrainment ratio increases with decrease of secondary fluid pressure (i.e. evaporator pressure), while it increases with increase of generator temperature, at constant evaporator temperature and condenser pressure.
- Below the critical values of condenser pressure, the entrainment ratio remains unaffected with the condenser pressure.
- The ejector -based vapour absorption cycle has better performance than the basic absorption cycle for evaporator temperature ranging from $2-10°C$. The COP of the basic single effect LiBr/water cycle increased by 45% on incorporation of ejector.

NOMENCLATURE

CFD	Computational Fluid Dynamics	(-)
COP	Coefficient of Performance	(-)
ER	Entrainment ratio	(-)
$\dot{m}_s$	Secondary Mass flow rate	(kg/s)
$\dot{m}_p$	primary Mass flow rate	(kg/s)
Mw	Molecular weight	(kg/kmol)
P	Pressure	(Pa)
Q	Heat	(W)
T	temperature	(K)
UDF	User-defined Function	(-)
ρ	density	(kg/m^3)
Ui	velocity	(m/s)
τ_{ij}	stress tensor	(-)
x, y, z	coordinates	(-)
α	thermal conductivity	(W/m-K)
μ	dynamic viscosity	(kg/m-s)
k	turbulent kinetic energy	(J)
δij	Kronecker symbol	(-)

Subscripts

C	Condenser
E	Evaporator
Eff	Effective
G	Generator
i,j	space components
P	Primary flow
S	secondary flow

VII. REFERENCES

[1] P. Srikhirin and S. Chungpaibulpatana, (2001), A review of absorption refrigeration technologies, Renew. Sustain. Energy Rev. 5 (2001) 343–372
[2] D.S. Ward. Solar absorption cooling feasibility, Sol. Energy 22 (1979) 259–268
[3] J. M. Abdulateef, K. Sopian and M. A. Alghoul, (2009), Review on solar- driven ejector refrigeration technologies, Renew. Sustain. Energy Rev.13, pp1338–1349
[4] M. Sokolov and A. Arbel, (2004), Revisiting solar-powered ejector air conditioner – the greener the better, Sol. Energy 77, pp57–66
[5] Y. Ali, R. Sirwan and K. Sopian, (2013), Evaluation of adding flash tank to solar combined ejector–absorption refrigeration cycle, Sol. Energy 91, pp283–296
[6] H. Chen, J. Yu and Y. Ren, (2006), A new eject or refrigeration system with an additional jet pump, Appl. Therm. Eng. 26, pp.312– 319.
[7] M. Alghoul, Y. Ali, R. Sirwan, (2013), Thermodynamic analysis of an ejector- flash tank-absorption cooling system, Appl. Therm. Eng. 58, pp 85–97.
[8] A. M. Abed, M. A. Alghoul and A. N. Al-Shamani, (2015), Performance enhancement of ejector–absorption cooling cycle by re-arrangement of solution streamlines and adding RHE, Appl. Therm. Eng. 77, pp.65–75
[9] A. N. Al-Shamani, A. M. Abed, (2015), Evaluating ejector efficiency working under intermediate pressure of flash tank–absorption cooling cycle: parametric study, Chem. Eng. Process 95, pp.222–234.
[10] Hasan Sh. Majdi, (2016) Performance evaluation of combined ejector LiBr/H2O absorption cooling cycle, Case Studies in Thermal Engineering, Elsevier, 7 (2016), 25-35, Al-Mustaqbal University College, Babylon, Iraq
[11] ASHRAE, (1979), Steam-Jet Refrigeration Equipment, Equipment Handbook, vol.13, pp. 13.1-13.6
[12] ESDU, (1986), Ejectors and Jet Pumps, Design for Steam Driven Flow, Engineering Science Data item 86030, Engineering Science Data Unit, London.
[13] J.M. Chang, B.J. Huang, C.P. Wang, A (1999), 1-D Analysis of Ejector Performance, International Journal of Refrigeration, vol. 22, pp. 354–364.
[14] B.J. Huang, R.H. Yen, C.Y. Chen, and K. Shestopalov, (2013), Performance Optimization for a Variable Throat Ejector in a Solar Refrigeration System, International Journal of Refrigeration, vol. 36, pp. 1512-1520.
[15] P. Jiang and Y. Zhu, Hybrid (2012) Vapour Compression Refrigeration System with an Integrated Ejector Cooling Cycle, International Journal of Refrigeration, vol. 35, pp. 68-78.
[16] P. A. Desevaux , Y. Bartosiewicz and Z. Aidoun, (2005), Numerical and Experimental Investigations on Supersonic Ejectors," International Journal of Heat and Fluid Flow, vol. 26, pp. 56–70.

[17] S. A. Mohamed, M. N. Karimi, (2020). Analysis and Optimization of vapor absorption generator-heat exchanger using Kern method and CFD. Journal of Thermal Engineering, Vol. 6, No. 4, pp. 440-459.
[18] S. A. Mohamed and M. N. Karimi, Simulation of Lithium Bromide- Water (LiBr-H_2O) Vapor Absorption System (VAS) powered by Solar Flat Plate Collector (SFPC). IOP Conference Series: Materials Science and Engineering. vol. 691 (2019) 012031.
[19] H. Havtun and J. Chen, (2014), Investigation of Ejectors in Refrigeration System: Optimum Performance Evaluation and Ejector Area Ratios Perspectives, Applied Thermal Engineering, vol. 64, pp. 182-19.
[20] C. Bouden and Y. Allouche, (2013), A CFD Analysis of the Flow Structure inside a Steam Ejector to Identify the Suitable Experimental Operating Conditions for a Solar-driven Refrigeration System International Journal of Refrigeration, vol. 30, pp. 1-10.

.